

## Supplementary Information

for

### Development of photochemical and electrochemical cells for *operando* X-ray absorption spectroscopy during photocatalytic and electrocatalytic reactions

Rachit Khare<sup>a</sup>, Andreas Jentys<sup>a,\*</sup>, and Johannes A. Lercher<sup>a,b</sup>

<sup>a</sup> Department of Chemistry and Catalysis Research Center, Technical University of Munich, Garching, Germany.

<sup>b</sup> Institute for Integrated Catalysis, Pacific Northwest National Laboratory, Richland, USA.

\* Corresponding author (Email: [jentys@tum.de](mailto:jentys@tum.de))

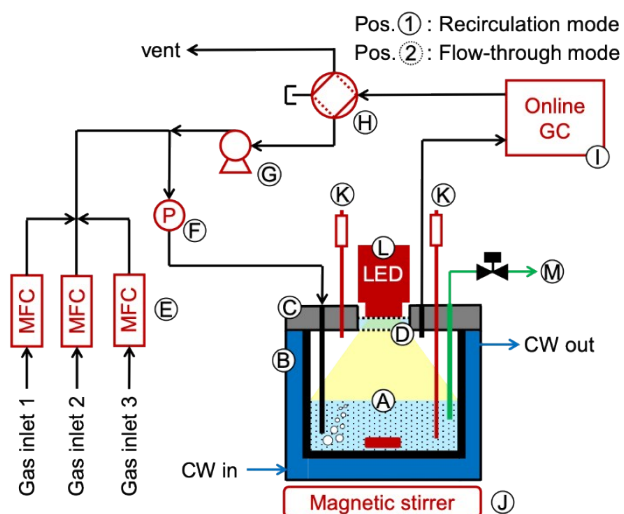


**Fig. S1** Gas-dosing and recirculation setup for conventional photocatalytic reactions. (A) top-irradiated batch-type PTFE photoreactor, (B) aluminum cooling jacket connected to a recirculating chiller unit (Julabo), (C) PTFE reactor cover with several inlet and outlet ports, (D) UV/vis transparent quartz window (Edmund Optics), (E) mass flow controllers (Bronkhorst), (F) pressure meter (Bronkhorst), (G) double diaphragm gas pump (KNF Neuberger), (H) switching valve (VICI Valco), (I) online GC (Shimadzu 2010 Plus), (J) magnetic stirrer (ThermoFischer), (K) K-type thermocouples (Omega), (L) UV or visible light LED lamp equipped with an optical guide and a collimator lens (Prizmatix), and (M) liquid sampling port.

## S1 Catalyst characterization

**S1.1 Elemental analyses.** Metal concentrations were determined by inductively coupled plasma–atomic absorption spectroscopy (ICP–AAS) using a Thermo Scientific–SOLAAR M Series AA spectrometer. Hydrogen-, carbon-, and nitrogen- elemental analyses were carried out by the Microanalytical Laboratory of the Catalysis Research Center, Technical University of Munich. Elemental compositions of the as-synthesized bulk g-C<sub>3</sub>N<sub>4</sub> and g-C<sub>3</sub>N<sub>4</sub>-ns are shown in Table S1. A higher hydrogen content than the theoretical value corresponds to incomplete thermal polymerization of dicyandiamide possibly resulting in the formation of intralayer hydrogen bonds in the graphite-like material.

**Table S1** Elemental composition (carbon-, nitrogen-, and hydrogen- content, in wt.-%) of bulk g-C<sub>3</sub>N<sub>4</sub> and g-C<sub>3</sub>N<sub>4</sub>-ns. The elemental composition reported is adjusted for water content in the material (4.1 wt.-% in bulk g-C<sub>3</sub>N<sub>4</sub> and 3.5 wt.-% in g-C<sub>3</sub>N<sub>4</sub>-ns). Theoretical elemental composition of pure graphitic carbon nitride is also shown.

	C /wt.-%	N /wt.-%	H /wt.-%	Stoichiometric formula
g-C <sub>3</sub> N <sub>4</sub> (theoretical)	39.1	60.9	-	C <sub>3</sub> N <sub>4</sub>
Bulk g-C <sub>3</sub> N <sub>4</sub>	35.4	62.8	1.84	C <sub>3</sub> N <sub>4.55</sub> H <sub>1.86</sub>
g-C <sub>3</sub> N <sub>4</sub> -ns	35.4	62.8	1.77	C <sub>3</sub> N <sub>4.55</sub> H <sub>1.82</sub>

**S1.2 Textural properties.** Specific surface areas of bulk g-C<sub>3</sub>N<sub>4</sub>, g-C<sub>3</sub>N<sub>4</sub>-ns, and TiO<sub>2</sub>, were determined by N<sub>2</sub> adsorption-desorption measurements carried out at 77 K using a Quantachrome NovaTouch 4.x Gas Sorption Analyzer. All samples were outgassed at 523 K for 3 h before adsorption-desorption measurements. The specific surface area was calculated via the Brunauer-Emmett-Teller (BET) method. Fig. S2 shows the results of N<sub>2</sub> adsorption-desorption measurements. The surface area of TiO<sub>2</sub> was estimated to be 69 m<sup>2</sup>·g<sup>-1</sup> while that of bulk g-C<sub>3</sub>N<sub>4</sub> was 43 m<sup>2</sup>·g<sup>-1</sup>. The surface area of bulk g-C<sub>3</sub>N<sub>4</sub> increased significantly to ~130 m<sup>2</sup>·g<sup>-1</sup> on thermal treatment. This suggests that the thermal treatment exfoliated the bulk material to form g-C<sub>3</sub>N<sub>4</sub> nanosheets with higher surface area.

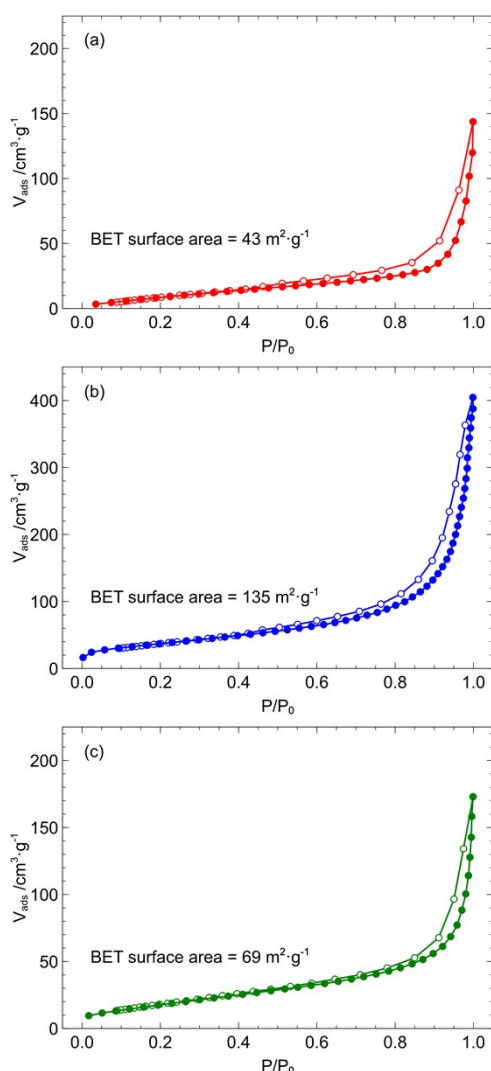


**Fig. S2** N<sub>2</sub> adsorption (closed symbols) and desorption (open symbols) measurements on (a) bulk g-C<sub>3</sub>N<sub>4</sub> (red), (b) g-C<sub>3</sub>N<sub>4</sub>-ns (blue), and (c) TiO<sub>2</sub> (green), at 77 K. The calculated surface areas using the Brunauer-Emmett-Teller (BET) method are also reported.

**S1.3 Powder X-ray diffraction (XRD).** Powder XRD patterns were collected on a Malvern Panalytical Empyrean diffractometer equipped with a Cu X-ray tube (Cu-K $\alpha$ )

radiation, 0.154 nm), a Ni K $\beta$ -filter, and a solid-state detector (X'Celerator), operated at 45 kV and 40 mA. Measurements were performed between 5° and 70° (for bulk g-C<sub>3</sub>N<sub>4</sub> and g-C<sub>3</sub>N<sub>4</sub>-ns) or between 5° and 90° (for TiO<sub>2</sub>) with a scan step size of 0.013° and a scan time of 60 s per step. The XRD patterns are shown in Fig. S3. The characteristic peaks associated with graphitic carbon nitride are also shown. The peak at  $2\theta = 27.4^\circ$ , equivalent to a  $d$ -spacing of 0.326 nm, can be ascribed to the interlayer distance in the graphitic material.<sup>1, 2</sup> The peak at  $2\theta = 13.0^\circ$ , corresponding to a  $d$ -spacing of 0.680 nm, is attributed to intralayer  $d$ -spacing.<sup>1, 2</sup> The characteristic peaks associated with anatase ( $2\theta = 25.3^\circ, 48.1^\circ, \text{ and } 37.8^\circ$ ) and rutile ( $2\theta = 27.5^\circ, 54.5^\circ, \text{ and } 36.2^\circ$ ) phases of TiO<sub>2</sub> are also shown in Fig. S3.<sup>3, 4</sup>

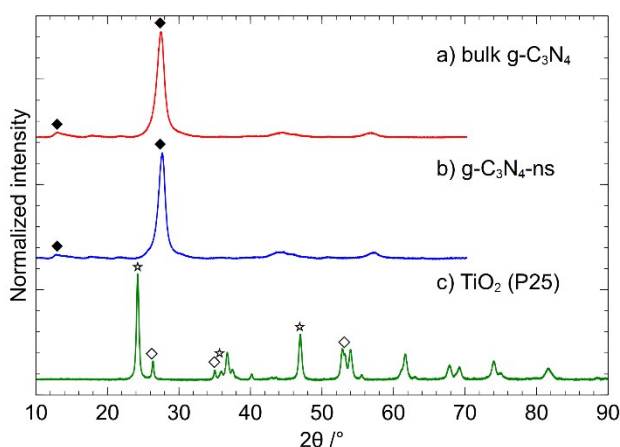


**Fig. S3** Powder XRD patterns of (a) bulk g-C<sub>3</sub>N<sub>4</sub> (red), (b) g-C<sub>3</sub>N<sub>4</sub>-ns (blue), and (c) TiO<sub>2</sub> (green). Characteristic peaks of graphitic carbon nitride (◆), and anatase (☆) and rutile (◇) phases of TiO<sub>2</sub>, are also shown.

**S1.4 UV-visible diffuse reflectance spectroscopy (UV-vis DRS).** UV-vis DRS measurements were performed with an Avantes Avaspec 2048 spectrometer equipped with a reflection probe (FCR-7UV200-2-ME) and a custom-made PTFE sample holder. For analyses, the Kubelka-Munk (K-M) functions ( $F(R_\infty)$ ) were calculated from reflectance ( $R_\infty$ ) as follows:

$$F(R_\infty) = \frac{(1 - R_\infty)^2}{2R_\infty}$$

The reflectance ( $R_\infty$ ) is defined as

$$R_\infty = \frac{R_{ref}}{R_{sample}}$$

where  $R_{sample}$  is the reflectance of the sample and  $R_{ref}$  is the reflectance of PTFE. The band gap energy ( $E_g$ ) and absorption coefficients are related through the well-known Tauc relations and  $E_g$  was estimated accordingly from Tauc plots ( $[F(R_\infty) \cdot hv]^{0.5}$  versus  $hv$ ). The results of UV-vis DRS measurements are shown in Fig. S4. The  $E_g$  of  $\text{TiO}_2$  was estimated to be 3.24 eV (383 nm) suggesting that it can be activated by the UV light. On the other hand, bulk  $\text{g-C}_3\text{N}_4$  and  $\text{g-C}_3\text{N}_4$ -ns have an  $E_g$  of 2.73 eV (454 nm) and 2.79 eV (444 nm), respectively, and therefore these materials can be activated by visible light.

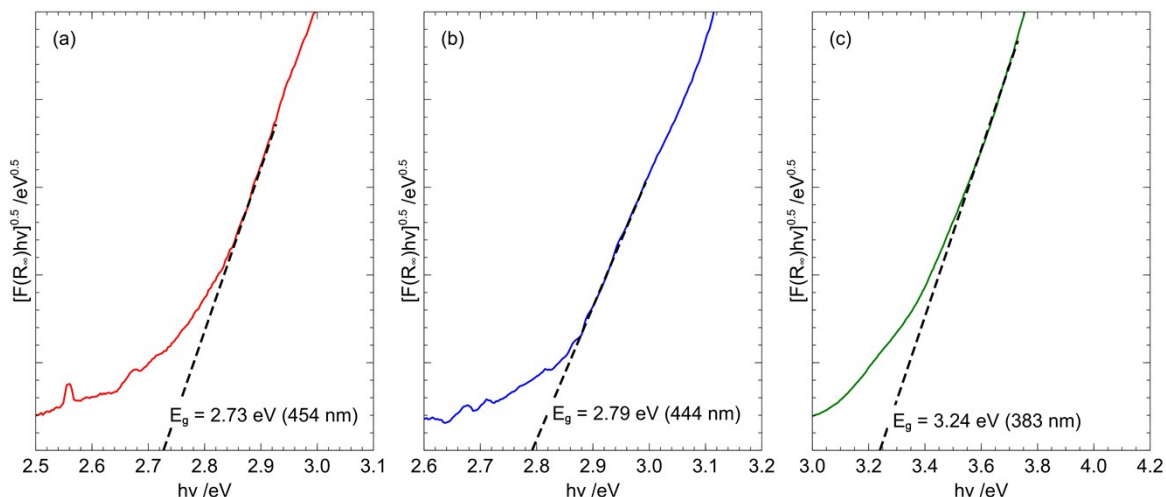


**Fig. S4** Tauc plots obtained from UV-vis DRS measurements on (a) bulk  $\text{g-C}_3\text{N}_4$  (red), (b)  $\text{g-C}_3\text{N}_4$ -ns (blue), and (c)  $\text{TiO}_2$  (green). The calculated band gap energy and the corresponding wavelengths (in parentheses) are also reported.

## S2 Photo-electrochemical setup

With a few modifications, the electrochemical cell together with a modified gas-dosing and gas/liquid-recirculation setup can be used for *operando* XAS measurements during photo-electrochemical experiments. Fig. S5 shows a schematic of the *operando* photo-electrochemical cell. The cell comprises of a working electrode and a counter electrode chamber separated by an ion-exchange membrane. The working electrode cover features two ports for inlet and outlet of the electrolyte and one port for inserting the reference electrode. The counter electrode cover also features two ports for the inlet and outlet of the electrolyte and a UV/vis transparent quartz window for providing illumination using an LED lamp. The cell features a glassy carbon window coated with an electrocatalyst as a working electrode and a similar counter electrode. The glassy carbon electrodes were connected to a voltage supply unit using titanium electrical connectors. The cell also features flow paths constructed out of 2 mm thick PTFE sheets for the working electrode and counter electrode chambers. The cell was sealed using rubber gaskets and stainless-steel nuts and bolts.

A schematic of the modified gas-dosing and gas/liquid-recirculation setup for photo-electrochemical experiments is shown in Fig. S6. The setup features two electrolyte reservoirs for the working-electrode and the counter-electrode chambers, respectively. The reservoirs are constructed out of PTFE and feature several ports for gas/liquid inlet and outlet. The reservoirs are enclosed inside aluminum cooling jackets connected to a recirculating chiller unit. The electrolyte was recirculated between the reservoirs and the *operando* electrochemical cell using liquid gear pumps. Gases were supplied to the reservoirs using mass flow controllers. A switching valve was used to switch between recirculation mode and flow-through mode. Temperature of the liquid and gas phase was monitored using K-type thermocouples. The pressure was continuously monitored using pressure meters. The electrolyte reservoirs also feature ports for sampling the liquid during the reaction for further analyses. Illumination was provided by a UV (365 nm 5 W) or visible (405 nm 4.4 W) LED lamp connected to a fiber-optic guide.

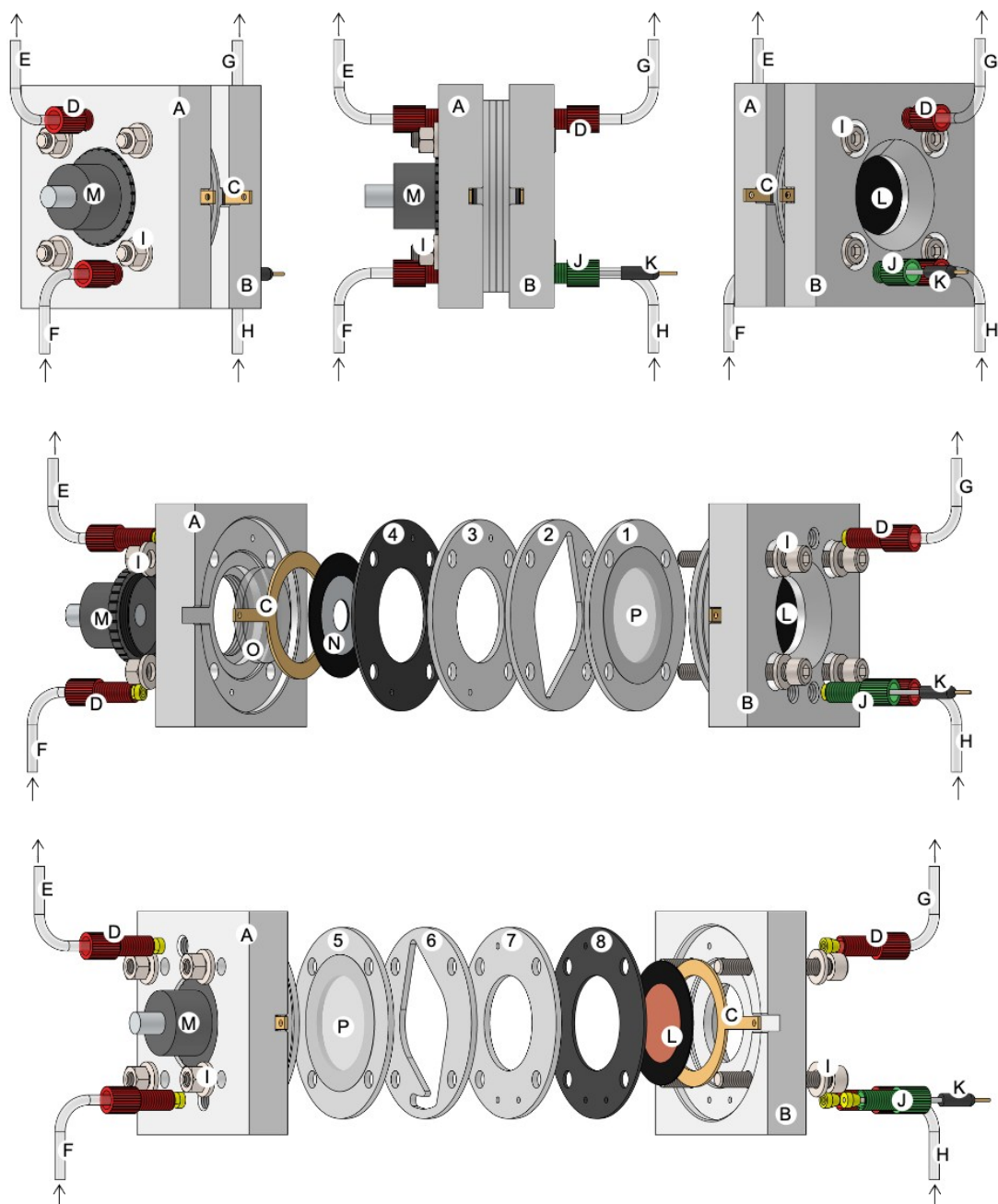


**Fig. S5** Cell design for *operando* XAS measurements during photo-electrocatalytic reactions. (A) PTFE counter-electrode cover, (B) PTFE working-electrode cover, (C) titanium electrical connectors, (D) PEEK flangeless fittings (IDEX OptoFluidic Systems), (E–F) PTFE electrolyte inlet and outlet for counter-electrode chamber, (G–H) PTFE electrolyte inlet and outlet for working-electrode chamber, (I) stainless steel nuts, bolts, and washers, (J) PEEK flangeless fitting (IDEX OptoFluidic Systems), for (K) Ag/AgCl leakless reference electrode (eDAQ), (L and N) 500  $\mu\text{m}$  thick glassy carbon window (HTW Germany) coated with electrocatalyst, (M) UV or visible LED lamp equipped with a fiber-optic guide (Prizmatix), (O) UV/vis transparent quartz window (Edmund Optics), (P) Nafion® perfluorinated ion-exchange membrane (Sigma-Aldrich), (1–3) flow path for working-electrode chamber constructed out of 2 mm thick PTFE sheets (Garlock), (5–7) flow path for counter-electrode chamber constructed out of 2 mm thick PTFE sheets (Garlock), and (4 and 8) rubber sealing gaskets.

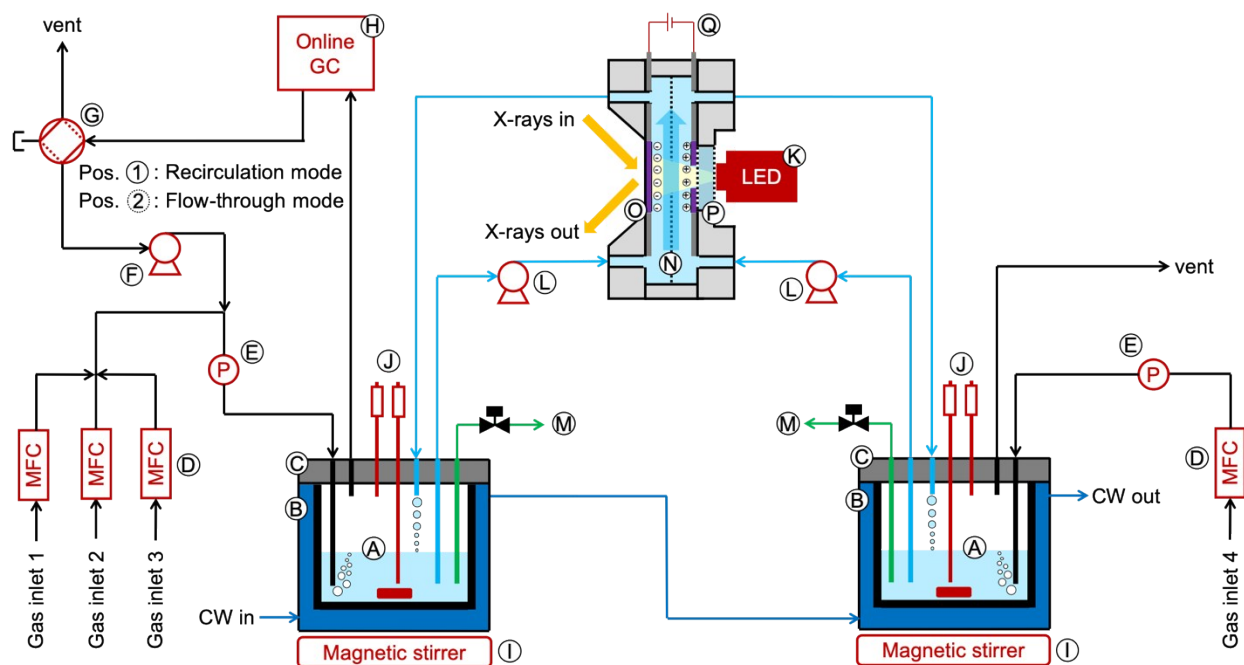


**Fig. S6** Gas-dosing and gas/liquid-recirculation setup for *operando* XAS measurements for photo-electrocatalytic experiments. (A) PTFE electrolyte reservoirs, (B) aluminum cooling jacket connected to a recirculating chiller unit (Julabo), (C) PTFE lid with several inlet and outlet ports, (D) mass flow controllers (Bronkhorst), (E) pressure meters (Bronkhorst), (F) double diaphragm gas pump (KNF Neuberger), (G) switching valve (VICI Valco), (H) online GC (Shimadzu 2010 Plus), (I) magnetic stirrer (ThermoFischer), (J) K-type thermocouples (Omega), (K) UV or visible LED light source equipped with an optical guide (Prizmatix), (L) liquid gear pumps (Ismatec), (M) liquid sampling ports, (N) Nafion® perfluorinated proton-exchange membrane (Sigma-Aldrich), (O) 500  $\mu\text{m}$  thick glassy carbon window (HTW Germany) coated with electrocatalyst, (P) UV/vis transparent quartz window (Edmund Optics), and (Q) voltage supply unit (BioLogic VSP-300).

## References

1. F. Fina, S. K. Callear, G. M. Carins and J. T. S. Irvine, *Chemistry of Materials*, 2015, **27**, 2612-2618.
2. X. Wang, K. Maeda, A. Thomas, K. Takanabe, G. Xin, J. M. Carlsson, K. Domen and M. Antonietti, *Nature Materials*, 2009, **8**, 76-80.
3. R. T. Downs and M. Hall-Wallace, *American Mineralogist*, 2003, **88**, 247-250.
4. C. J. Howard, T. M. Sabine and F. Dickson, *Acta Crystallographica Section B*, 1991, **47**, 462-468.